Effect of Manufacturing Techniques in Pressure Drop on Triple Periodical Minimal Surface Packings

Arthur Zimmer[1], José D. Pacheco Araújo[2], Kari Anne Andreassen[1], and Carlos A. Grande[1,*]

DOI: 10.1002/cite.202000237

Supporting Information available online

In Memory of Prof. Dr.-Ing. Jens Weitkamp

Structured packings are important elements to enhance mass and heat transfer in the chemical industry. New techniques of manufacturing, like 3D printing, can create completely new families of solids used for this purpose. In this work the effect of different 3D printing techniques in the manufacture of packings with triply periodic minimal surfaces (TPMS) geometry was analyzed and the influence of different 3D printing techniques in the final properties of packings produced with TMPS topologies, both numerically and experimentally, were studied.

Keywords: 3D printing, CFD, Pressure drop, Structured packing, Triply periodic minimal surfaces

Received: November 07, 2020; *revised:* December 23, 2020; *accepted:* February 09, 2021

1 Introduction

Process intensification of separation and reaction processes can be achieved by increasing the internal contact area [1, 2]. Such contact area can be used for promoting reaction/adsorption, increasing mass transfer or heat transfer, and is normally bounded by constraints in pressure drop. Internal packings are used in almost all absorption and distillation processes to enhance gas-liquid contact. A common example practised for almost a century, is to pack columns with structures like Raschig rings [3, 4]. These structures fill the column homogeneously and render a rather uniform porosity all across the column. For this reason, although these packings may be manufactured with a well-tailored design, it is possible to visualize them as a 1D packing (due to uniform porosity and homogeneous heat transfer properties). Novel designs of random packings can achieve rather high surface area per volume but in such cases, the main limitation is that they cannot be used at high flowrates.

In 1940's, structured packings were developed and since then, they have dominated the market of packings [5, 6]. These structured packings are manufactured by joining several 2D patterned sheets in parallel that are adapted to a geometry by wrapping them up by an external network. The different patterns render different properties of mixing and of surface area. It is normal practice also to increase the rugosity of the sheets to achieve higher surface area per unit volume of solid. The major advantage introduced by these 2D structured packings was a much higher surface area per volume of material for an equivalent pressure drop. Also, the structured packings will not fluidize and thus can be used at higher flowrates than the random packings. One very good scenario of the dominance of structured packings is in the three-way car catalysts, where only honeycomb monoliths are used nowadays [7].

Given the enhancement of process intensification achieved when moving from 1D packings to 2D packings, we also expect that when using three-dimensional arrays, better packing properties can be achieved. Additionally, such 3D designs can also be tailored for using them as mass transfer agents (like in absorption and distillation) or as heat transfer elements in reactors in completely different applications [8–14].

Three-dimensional (3D) printing consists in producing a 3D structure from a model, created in a CAD (computer

[1]Arthur Zimmer, Kari Anne Andreassen, Dr. Carlos A. Grande
carlos.grande@sintef.no
SINTEF AS, Forskningsveien 1, 0373 Oslo, Norway.

[2]Dr. José D. Pacheco Araújo
Centro de Estudos de Fenómenos de Transporte, Departamento de Engenharia Química, Faculdade de Engenharia da Universidade do Porto, Rua Dr. Roberto Frias, 4200-465 Porto, Portugal.

aided design) software using mathematical equations, solid modelling or from scans of imaging technologies. The object to be manufactured is produced by depositing the material layer-by-layer. This "positive" methodology for constructing an object provides additional flexibility for manufacturing when compared to existing "subtractive" manufacturing technologies. There are manufacturing limitations in 3D printing, that depend strongly on the technique used. The statement that 3D printing can manufacture all types of objects is perhaps overrated, but it is important to stress that in most cases, the design of an object can be tuned to be printable while keeping a large portion of its features. An important benefit of 3D printing is that when creating complex objects layer-by-layer, the amount of waste is much smaller than the one obtained when producing a similar object by subtractive techniques. In this work, three different 3D printing technologies were used to produce the same object: stereolithography (SLA), selected laser sintering (SLS), and multi jet fusion (MJF).

Stereolithography (SLA) is based on the solidification of a liquid resin by photo-polymerization using a laser. The resins normally used are composed of polyacrylates and a polymerization initiator that polymerize fast upon being in contact with the laser. This technology is nowadays very popular, and its cost has been dramatically reduced. It has a good finishing, and it is possible to print in a scale of tens of centimeters with a $\sim$50 µm *xy* resolution.

Selective laser sintering (SLS) is another 3D printing technique that generates objects by sintering a powder with a laser (fusing the material). The standard powders used are thermoplastics like nylon or polyamide. The laser intensity is modulated to ensure that the new layer is bonded to the layer beneath and to facilitate that, the powdered bed is also pre-heated. The *xy* resolution is also on the tens of microns. SLS technology does not need to use supports to hold the structures to be printed. This is an important advantage once that many designs can be printed without generating any rubbish and because the entire volume of the printer can be used for printing objects.

Multi Jet fusion (MJF) is a 3D printing technique developed by HP where an ink (that acts as a fusing agent) is dispensed on the powder that will constitute the solid. The ink helps fusing the powder by promoting absorption of infrared light that is given by an external source. The material used should also be a thermoplastic and the resolution is thus given by the granulometry of the powder used, as in SLS.

In this work small-structured packings (that can be fitted in a one-inch external column diameter) based on a Schwartz diamond TPMS function with different cell sizes and thus rendering different porosities and surface area to volume ratios are produced. Moreover, our target was to evaluate the importance of the 3D printing technique in producing the packings. We have measured pressure drop through these packings for single-phase flow (air at 20 °C) at different velocities addressing both laminar and turbulent flow regimes. Simulations were also performed with computational fluid dynamics (CFD) tools that provided numerical data for comparison with the experimental results in the laminar regime.

2 Experimental

2.1 Design and Manufacturing of TPMS Packings

Triply periodic minimal surfaces (TPMS) are mathematical functions with zero curvature which means they are equally concave and convex in all points. They represent a periodic structure in three directions characterized by a continuous geometry and connectivity of the sub-cells that constitute the structure. These structures are inspired by natural geometries and have good properties such as high porosity and high mechanical strength. In 1970, Alan Schoen named these structures, being the Schwarz primitive (P), Schwarz diamond (D), and Schwarz gyroid (G) the most common. The mathematical function of the Schwartz diamond is:

$$\begin{aligned}&\sin\left(\frac{\pi x}{\delta}\right)\sin\left(\frac{\pi y}{\delta}\right)\sin\left(\frac{\pi z}{\delta}\right)\\&+\sin\left(\frac{\pi x}{\delta}\right)\cos\left(\frac{\pi y}{\delta}\right)\cos\left(\frac{\pi z}{\delta}\right)\\&+\cos\left(\frac{\pi x}{\delta}\right)\sin\left(\frac{\pi y}{\delta}\right)\cos\left(\frac{\pi z}{\delta}\right)\\&+\cos\left(\frac{\pi x}{\delta}\right)\cos\left(\frac{\pi y}{\delta}\right)\sin\left(\frac{\pi z}{\delta}\right)=\gamma\end{aligned} \tag{1}$$

where δ is the wavelength of each of the diamond cells and γ is the iso-surface correction term, normally set to zero. Reducing the wavelength results in smaller cells and thus a higher surface area to volume ratio at the expense of a lower bed porosity and thus a higher pressure drop. Once that a surface with this function is obtained, it has to be thickened with a width dimension (σ) to obtain a packing with a finite volume.

In this work, the TPMS were generated using the Axolotl plugin for Grasshopper, which is a parametric toolbox in Rhinoceros (McNeel & Assoc. USA). The plugin is based on a volumetric modelling approach described in detail elsewhere [15]. The plugin allows a rather straightforward generation of a variety of TPMS solids having a wavelength (δ), the thickness of the layers (σ) and a resolution parameter as the main variables. When the resolution parameter is increased, a very smooth surface is obtained, at the expense of the generation of very large files so a compromise situation should be reached. This compromise has a direct impact on the final surface and volume of the solid also. An example of the effect of the resolution parameter in the generation of a single cell of the diamond structure is shown in Tab. 1. A visual representation of the single cells is shown in the Supporting Information.

The design parameters for all the packings used in this work were fixed. A domain radius of 10.45 and a length of

Table 1. Effect of the design parameters of diamond TPMS in surface properties and file size.

Wavelength δ	Resolution	Thickness σ	Surface area	Volume	File size
[mm]	[mm]	[mm]	[mm^2]	[mm^3]	[kB]
7	0.45	0.25	149.99	19.87	121
7	0.40	0.25	151.39	23.59	156
7	0.30	0.25	160.74	26.55	270
7	0.20	0.25	173.37	28.91	669
7	0.15	0.25	179.46	29.94	1211
7	0.10	0.25	185.79	31.00	2796
8	0.20	0.49	243.60	82.46	922
4	0.20	0.47	53.16	8.60	212
2	0.20	0.48	6.90	0.42	32

19.6 mm were used with a voxel resolution of 0.2 mm. Three different wavelengths were used: 8, 4 and 2 with the layer thickness of 0.49, 0.48 and 0.47, respectively. The layer thickness was slightly changed to fix the design porosity to 0.60, 0.70 and 0.80, respectively. The different modules were manufactured with three different 3D printing techniques: oligomeric material (clear resin in SLA (Formlabs 1+, USA), SLS (PA12 in SnowWhite, Shareboot, Italy) and MJF (Polyamide in HP, USA). Many different modules were produced by all the techniques and the results presented here have very small variations with different samples (were repeated at least twice). Images of the different modules (20 mm length) are given in Fig. 1. The image of all the modules is shown in the Supporting Information as well as some experiments made to show reproducibility. Note that we have also produced some larger modules with 40 and 60 mm length. The list of parameters used for the design of all the packings is listed in Tab. 2.

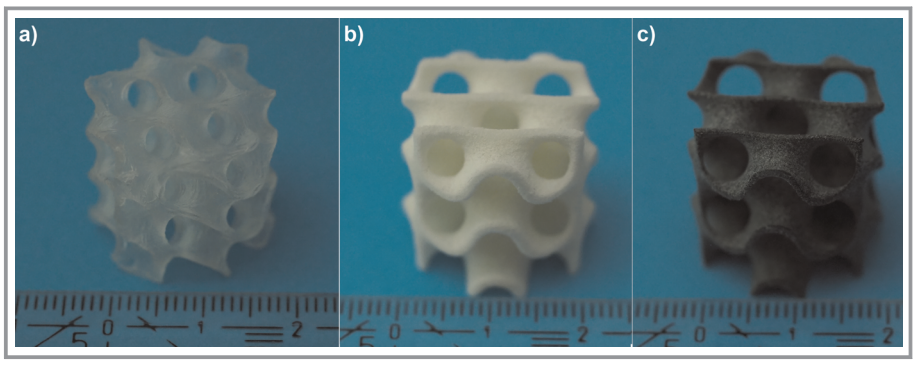

Figure 1. Diamond TPMS packings produced with a) SLA, b) SLS, and c) MJF. The solids have a diameter of 20.9 mm and a length of 19.6 mm.

2.2 Pressure Drop Measurements

The equipment used was inspired in other units published elsewhere [16]. All the experiments were made with compressed air from a distributed line at 20 °C. There are two mass flow controllers (Bronkhorst, Netherlands) to control the flow of air into the system in two different flow ranges: 0–4 SLPM and 0–50 SLPM. When the air exits the mass flow controllers (1/4-inch tube), it expands to a one-inch external diameter tube (21.1 mm internal diameter). After the expansion point, a one-inch tube with a length of 0.67 m is used to stabilize the flow pattern before the place where the packings are tested. Flow calibration was done with modules of a HORIBA STEC bubble units for different flowrates (0–1 SLPM, 0–10 SLPM, and 0–100 SLPM).

At the bottom of the column, a very porous metal mesh is fixed to hold the structures to be measured, although in this case is not required. The pressure drop of this mesh is 18 Pa at a velocity of 2 m s^{-1}, which is much smaller than the results with any of the samples used. A differential pressure sensor (Testo 435-4) is used to measure the pressure drop before the metal mesh and after the column where the packings are placed. A picture of the unit is given in the Supporting Information.

The measurements of pressure drop reported were collected in the superficial velocity range between 0–2.0 m s^{-1} and values were taken after at least one minute of constant reading.

3 Mathematical Modelling

CFD is a reliable and powerful complement to experimental techniques with important advantages like the flexibility and easiness to perform parametric studies at low costs, and the ability to produce relevant information with a higher level of detail and for very short time intervals. As a consequence, these numerical techniques have extensively proven their utility, not only in fundamental studies – e.g., in subjects like multiphase flow hydrodynamics [17] and heat and mass transfer [18] – but also in works with a practical nature such the ones involving the design and characterization of structured packings [19, 20].

Regarding CFD packages, for different reasons, users can choose to use commercial or open-source packages. To demonstrate that the generic approach of applying CFD modelling before manufacturing is not restricted to one of these options, simulations with COMSOL Multiphysics® and OpenFOAM® were performed.

Table 2. Design parameters used to produce diamond TPMS packings with different 3D printing techniques: SLA, SLS, and MJF.[a)]

Sample	3DP	Length+ [mm]	δ [mm]	σ [mm]	ε_c^{design} [–]	$\varepsilon_c^{exp\ b)}$ [–]	a_s [m^2m^{-3}]	Area [mm^2]	V_S [mm^3]
1	SLA	20.20	8.0	0.49	0.798	0.767	522.9	3583.39	1384.33
2		20.27	4.0	0.47	0.705	0.577	865.5	5931.73	2020.39
3		20.11	2.0	0.48	0.605	0.373	1071.1	7345.23	2706.56
4	SLS	20.16	8.0	0.49	0.798	0.797	522.9	3583.39	1384.33
5		20.22	4.0	0.47	0.705	0.695	865.5	5931.73	2020.39
6		20.23	2.0	0.48	0.605	0.602	1071.1	7345.23	2706.56
7	MJF	19.96	8.0	0.49	0.798	0.828	522.9	3583.39	1384.33
8		19.80	4.0	0.47	0.705	0.721	865.5	5931.73	2020.39
9		19.98	2.0	0.48	0.605	0.639	1071.1	7345.23	2706.56

a) The values reported are for design length of 19.6 mm and radius of 10.45 mm and resolution of 0.2 mm per voxel side. b) The value reported is experimentally measured.

In this work, CFD simulations of gas flow through a tube with 3D printed packings were performed for different average inlet velocities in laminar flow conditions. The governing equations applied to describe the system were the momentum and continuity equations (for incompressible flow) already implemented in both packages:

$$\frac{\partial\vec{\mathbf{u}}}{\partial t}+\nabla\left(\vec{\mathbf{u}}\vec{\mathbf{u}}\right)=-\nabla p+\nu\nabla\left(\nabla\vec{\mathbf{u}}\right) \tag{2}$$

$$\nabla\vec{\mathbf{u}}=0 \tag{3}$$

where $\vec{\mathbf{u}}$ denotes the velocity vector, p is the kinematic pressure (P/ρ) and ν is the kinematic viscosity (μ/ρ). The numerical details of the simulations are disclosed in the Supplementary Information.

4 Results and Discussions

4.1 Effect of Manufacturing

The packing units were designed with selected thickness parameters so that they can be manufactured with different 3D printing techniques (even on existing technological platforms). Moreover, the designs used in this work are directly scalable to larger modules. One of the purposes of the work was to understand the limitations of each 3D printing technology and the impact of the obtained properties in the packing materials. The solids with a length of 20 mm produced with the different printing techniques are shown in Fig. 1.

When the models are produced by stereolithography, they need supports. If the support removal is not done carefully, the small damages in the structure will result in a solid with slightly different properties as what is expected. This is more notorious in the solids with a smaller wavelength and in smaller structures. This can be improved by scaling up the models or alternatively, by adding an external wall. On the other side, the solid walls of the structures produced by SLA are smoother than the solids produced with SLS and MJF. The rugosity of the samples produced with the different techniques is shown in the Supplementary Information. In the samples printed with SLA it is possible to see the line-by-line production process with rugosities of ± 30 microns. It is fair to say that the results used in this work were produced with a rather old SLA printer. Results with an updated SLA printer (Form 3) produce much smoother parts as can be seen in the Supplementary Information. In the case of SLS and MJF the particles of the polymer are melted to form the objects and they are only partially melted in the superficial layer, bringing the rugosity to higher values in the order of ±40 microns.

4.2 Estimation of Pressure Drop Using CFD in Laminar Flow

One of the main advantages of using additive manufacturing for the design of packings, is that a CAD (or equivalent) file has to be done prior to manufacturing. This file can be used for modelling the performance of the design before is manufactured. There is different software that allow predictive modelling based on CAD designs to be used for 3D printing manufacturing and all have their pros and cons. The purpose of this work is not to disclose advantages or disadvantages of any particular software, but to highlight the flexibility of the approach of modelling before manufacturing. In this work, we have used OpenFoam and Comsol Multiphysics and simulations are in good agreement between the different software and also with the experimen-

tal data. From the pressure fields data, it was extracted the values for cross-section sliced immediately before and after the packing region. The average pressure was calculated for each of these slices and the difference between them gives the numerical result of the pressure drop through the packing module. This post-processing procedure was repeated for all simulated systems. In Fig. 2 the pressure and velocity vector fields are shown for the diamond TPMS with a wavelength of 2 mm (used for samples 3, 6 and 9).

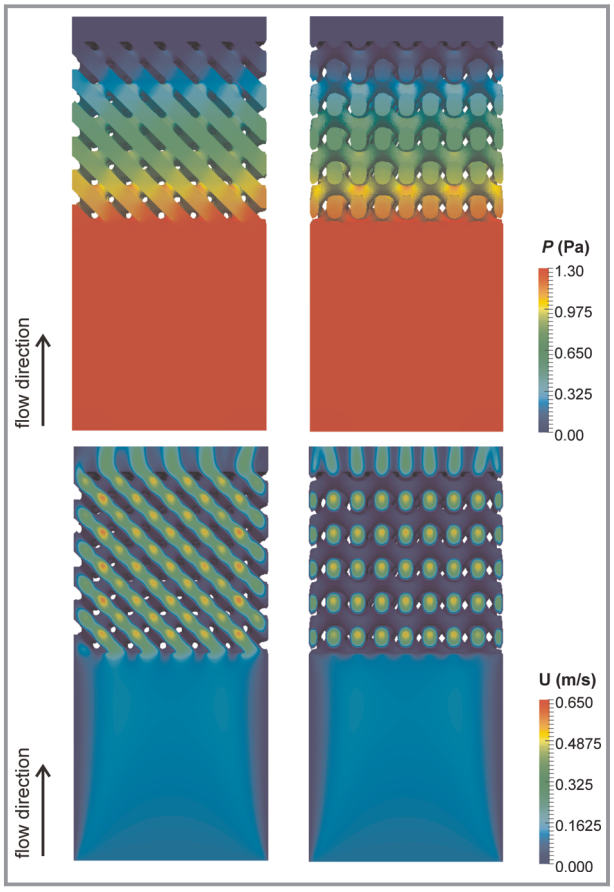

Figure 2. Pressure (upper figures) and velocity magnitude (lower figures) fields for the simulation with Model 3 packing and an inlet velocity of 0.1 m s^{-1}. The fields concern the views from two longitudinal cuts: frontal (left figures) and diagonal (right figures).

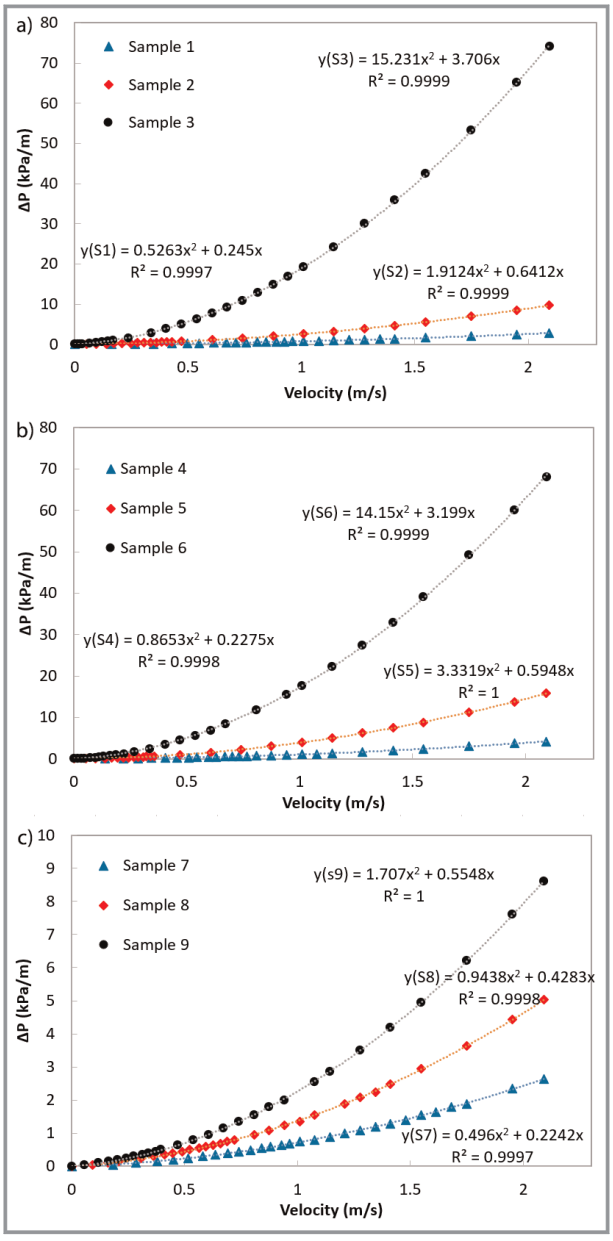

Figure 3. Pressure drop as a function of velocity for diamond TPMS packings produced with a) SLA, b) SLS, and c) MJF.

4.3 Measurement of Pressure Drop in Different Packings

The experimental results of pressure drop at different gas superficial velocities in the different samples is shown in Figs. 3 and 4. Note that the results in Fig. 3 are grouped according to the wavelength function and presented for the different techniques used. In Fig. 4, the results are arranged with a fixed function wavelength for the different 3D printing techniques. The log-log scale used in Fig. 4 is also shown to enhance the visualization in the low gas velocities region (laminar flow). In this figure, the results obtained by CFD are also included as the theoretical predictions. The pressure drop obtained in these TPMS structures is slightly higher than the one obtained using cubic lattice structures [10, 11]. This was expectable and should be counter-balanced with a higher degree of mixing obtained in the TPMS surfaces.

As mentioned before, each of the experimental techniques is subjected to an error. In this case, the experimental errors of 3D printing can be quantified in terms of packing porosity and in terms of rugosity. Measuring the porosity (in this case measuring the solid volume) using simple

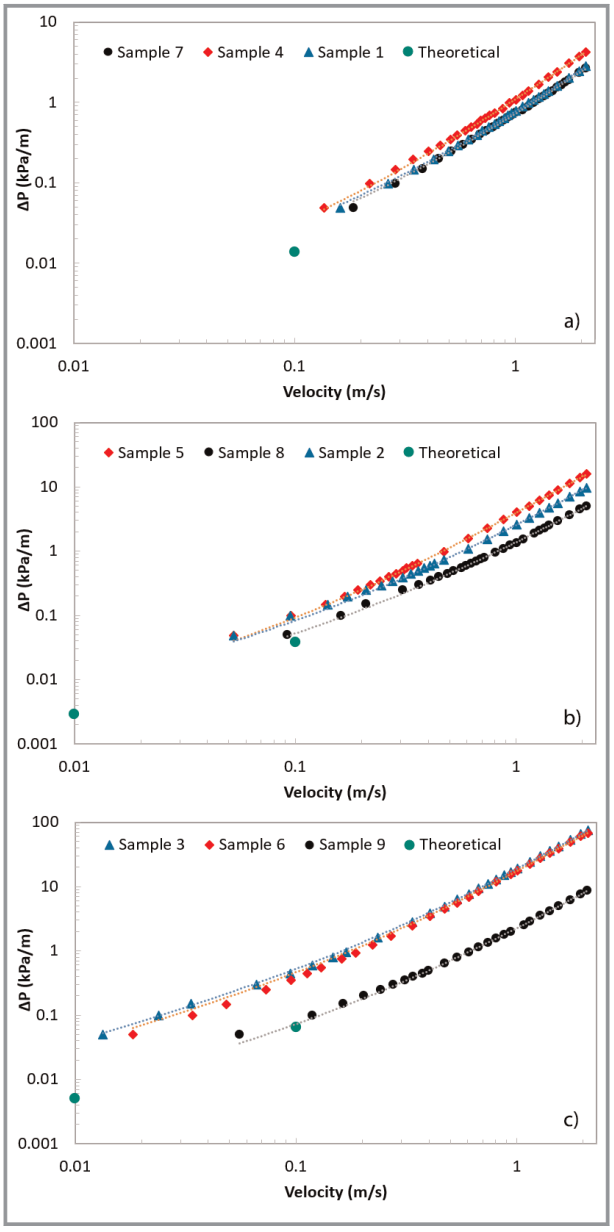

Figure 4. Log-log plot of pressure drop as a function of velocity for diamond TPMS packings produced with wavelength of a) 8.0 mm, b) 4.0 mm, and c) 2.0 mm.

techniques like water displacement, may be dangerous in case the sample is slightly porous. We have measured the displacement volume in a highly viscous oil that is not supposed to interact with any of the polymers used. The experimental values are reported in Tab. 2 and as can be seen, differ significantly for the different technologies used. In all the cases, the porosity is SLA < SLS < MJF. It should be noted that the results with a recent SLA machine may differ particularly due to an improved resolution in the machine and more controlled strategy for placing support structures. The results in the pressure drop are very sensitive to the porosity of the materials and thus the pressure drop obtained is normally higher for SLA materials followed by SLS. In the case of the samples with the smaller cells, the results with MJF are quite much smaller than with the other technologies and is again, due to the smaller porosity of the samples. On the turbulent regime, the experiments will also be able to reflect the rugosity of the sample [21]. In this case, it is also possible to see that the rugosity of the packings prepared with SLA are smoother than the other samples as shown in Fig. 2 and that is reflected in the pressure drop measurements.

There are several lessons to take from this study. The first one is that the large difference of the porosities obtained is related to the manufacturing technique but also, to a certain extent, to the design. In this case, a side voxel of 0.2 mm was used. Perhaps a larger file with 0.1 mm should be used for the manufacturing process, so that the slicing accuracy and the file dimensions at the *xy* coordinates are in agreement. The manufacture itself has several variables that should be optimized before producing TPMS solids that can also have a strong influence in the packing porosity. Ultimately, these variables have to be combined with corrosion studies for a given application and then decide which technique to be used and how the particular packings can be improved.

5 Conclusions

Structured packings with triply periodical minimal surfaces (TPMS) were designed and manufactured using three different type of 3D printing techniques: stereolithography (SLA), selective laser sintering (SLS) and multi jet fusion (MJF). Designs with three different porosities and surface area to volume ratio were done. The files used for the production using 3D printing technologies were also used for determining pressure drop in the laminar flow region. The produced packings were characterized in terms of rugosity and porosity. The porosity of the samples for the same files was always SLA < SLS < MJF. The rugosity also follows the same trend with the packings produced by SLA being smoother than the other units. We have used computational fluid dynamic simulations in two different software to demonstrate the generic approach of predicting before manufacturing can be applied to the design of such packings. Moreover, the experimental data obtained is in agreement with the simulation results in the laminar flow regime.

This work intends to communicate that the different 3D printing techniques do not only have material's variability, but also that the manufacturing techniques and the parameters for manufacturing should be well known before achieving a final product to be used for a given application. What is possible to observe in this study is that with simple geometric solids known from many years, it is possible to obtain very high surface area to volume ratios at high porosities.

We acknowledge the funding from the Research Council of Norway through the project 272729: New structured substrates for downstream processing of complex biopharmaceuticals. This project belongs to the m-era.net programme with Lithoz, IBET, Genibet and Cerpotech as partners. José D. P. Araújo acknowledges the financial support by: Base Funding – UIDB/00532/2020 and Programmatic Funding – UIDP/00532/2020 attributed to the Transport Phenomena Research Center – CEFT – financed by national funds through the FCT/MCTES (PIDDAC).

Symbols used

p	[$m^2 s^{-1}$]	kinematic pressure
$\vec{\mathbf{u}}$	[$m\ s^{-1}$]	velocity vector
ν	[$m^2 s^{-1}$]	kinematic viscosity

Greek symbols

γ	[mm]	iso-surface correction term
δ	[mm]	wavelength of each diamond cell
μ	[Pa s]	gas viscosity
ρ	[$kg\ m^{-3}$]	gas density

Abbreviations

CFD	computational fluid dynamics
MJF	Multi Jet Fusion
SLS	Selected Laser Sintering
SLA	Stereolithography
TPMS	triply periodic minimal surfaces

References

[1] P. C. Wankat, *Separation Process Engineering*, Prentice Hall, Boston **2007**.

[2] A. Stankiewicz, J. A. Moulijn, *Re-Engineering the Chemical Processing Plant*, Dekker, New York **2004**.

[3] N. Kolev, Packed Bed Columns. Elsevier, Amsterdam **2006**.

[4] P. Alix, J. Roesler, X. Courtial, M. Schultes. Hydraulic and Mass Transfer Performances of a Commercial Hybrid Packing: The RSP200X — Key Modelling Parameters for Gas Treatment Applications, *Chem. Eng. Res. Des.* **2019**, *147*, 597–602. DOI: https://doi.org/10.1016/j.cherd.2019.05.036

[5] A. Cybulski, J. A. Moulijn, *Structured Catalysts and Reactors*, CRC Press, Boca Raton, FL **2005**.

[6] F. Kapteijn, J. A. Moulijn. Structured Catalysts and Reactors – Perspectives for Demanding Applications, *Catal. Today*, in press. DOI: https://doi.org/10.1016/j.cattod.2020.09.026

[7] S. T. Gulati, Ceramic Catalysts Supports for Gasoline Fuel, in *Structured Catalysts and Reactors* (Eds: A. Cybulski, J. A. Moulijn), CRC Press, Boca Raton, FL **2005**.

[8] E. Miramontes, L. J. Love, C. Lai, X. Sun, C. Tsouris, Additively Manufactured Packed Bed Device for Process Intensification of CO_2 Absorption and Other Chemical Processes, *Chem. Eng. J.* **2020**, *388*, 124092. DOI: https://doi.org/10.1016/j.cej.2020.124092

[9] M. Bracconi, M. Ambrosetti, M. Maestri, G. Groppi, E. Tronconi, A Fundamental Analysis of the Influence of the Geometrical Properties on the Effective Thermal Conductivity of Open-Cell Foams. *Chem. Eng. Proc.* **2018**, *129*, 181–189. DOI: https://doi.org/10.1016/j.cep.2018.04.018

[10] M. Klumpp, A. Inayat, J. Schwerdtfeger, C. Körner, R. F. Singer, H. Freund, W. Schwieger, Periodic Open Cellular Structures with Ideal Cubic Cell Geometry: Effect of Porosity and Cell Orientation on Pressure Drop Behavior, *Chem. Eng. J.* **2014**, *242*, 364–378. DOI: https://doi.org/10.1016/j.cej.2013.12.060

[11] N. F. Bastos Rebelo, K. A. Andreassen, L. I. Suarez Ríos, J. C. Piquero Camblor, H.-J. Zander, C. A. Grande, Pressure Drop and Heat Transfer Properties of Cubic Iso-reticular Foams, *Chem. Eng. Proc.* **2018**, *127*, 36–42. DOI: https://doi.org/10.1016/j.cep.2018.03.008

[12] M. Lammermann, W. Schwieger, H. Freund, Experimental Investigation of Gas-Liquid Distribution in Periodic Open Cellular Structures as Potential Catalyst Supports, *Catal. Today* **2016**, *273*, 161–171. DOI: https://doi.org/10.1016/j.cattod.2016.02.049

[13] J. Stolaroff, High-Efficiency, Integrated Reactors for Sorbents, Solvents, and Membranes Using Additive Manufacturing, NETL CO_2 Capture Technology Meeting, Pittsburgh, August **2018**. https://netl.doe.gov/sites/default/files/netl-file/J-Stolaroff-LLNL-Reactor-Additive-Manufacturing.pdf

[14] D. W. Abueidda, M. Elhebeary, C.-S. Shiang, S. Pang, R. K. Abu Al-Rub, I. M. Jasiuk, Mechanical Properties of 3D Printed Polymeric Gyroid Cellular Structures: Experimental and Finite Element Study, *Mat. Design* **2019**, *165*, 107597. DOI: https://doi.org/10.1016/j.matdes.2019.107597

[15] M. Bernhard, M. Hansmeyer, B. Dillenburger, Volumetric Modelling for 3D Printed Architecture, in *Advances in Architectural Geometry* (Eds: L. Hesselgren, A. Kilian, O. Sorkine Hornung, S. Malek, K.-G. Olsson, C. J. K. Williams), Klein Publishing, Schorndorf **2018**, 392–415. https://research.chalmers.se/en/publication/504188

[16] A. Edouard, S. Ivanova, M. Lacroix, E. Vanhaecke, C. Pham, C. Pham-Huu, Pressure Drop Measurements and Hydrodynamic Model Description in SiC Foam Composites Decorated with SiC Nanofiber, *Catal. Today* **2009**, *141*, 403–408.

[17] J. D. P. Araújo, J. M. Miranda, J. B. L. M. Campos, Flow of Two Consecutive Taylor Bubbles Through a Vertical Column of Stagnant Liquid – A CFD Study About the Influence of the Leading Bubble in the Hydrodynamics of the Trailing One. *Chem. Eng. Sci.* **2013**, *97*, 16–33.

[18] M. C. F. Silva, J. D. P. Araújo, J. B. L. M. Campos, CFD Studies Coupling Hydrodynamics and Solid-Liquid Mass Transfer in Slug Flow for Matter Removal from Tube Walls. *AIChE J.* **2017**, *63 (6)*, 2420–2439.

[19] F. Lucci, A. Della Torre, J. v. Rickenbach, G. Montenegro, D. Poulikakos, P. D. Eggenschwiller, Performance of Randomized Kelvin-Cell Structures as Catalytic Substrates: Mass-Transfer Based Analysis, *Chem. Eng. Sci.* **2014**, *112*, 143–151.

[20] J. Sacher, J.-U. Repke, Development of a Mesoscale Model for the Gas Phase Fluid Dynamics in Structured Packings Based on Fundamental Experiments and CFD Investigations, *Chem. Eng. Res. Des.* **2019**, *147*, 430–442.

[21] T. P. Brackbill, S. G. Kandlikar, Effects of Roughness on Turbulent Flow in Microchannels and Minichannels, in *Proc. of the ASME 2008 6th Int. Conf. on Nanochannels, Microchannels, and Minichannels*, ASME. New York **2008**, 1179–1186. https://doi.org/10.1115/ICNMM2008-62224

